N85-22475

SHUTTLE ELECTRICAL ENVIRONMENT

M. Smiddy, W. P. Sullivan, D. Girouard
Air Force Geophysics Laboratory
Hanscom Air Force Base, Massachusetts 01731

P. B. Anderson
Regis College
Weston, Massachusetts

Part of an AFGL payload flown on the STS-4 mission consisted of experiments to measure in-situ electric fields, electron densities, and vehicle charging. During this flight some 11 hours of data were acquired ranging from 5 minute snapshots up to continuous half-orbits. These experiments are described and results presented for such vehicle induced events as a main engine burn, thruster firings and water dumps in addition to undisturbed periods. The main characteristic of all the vehicle induced events is shown to be an enhancement in the low frequency noise (less than 2 KHz), in both the electrostatic and electron irregularity ($\Delta N/N$) spectra.

The "non-event" results indicate that the electrostatic broadband emissions show a white noise characteristic in the low frequency range up to 2 KHz at an amplitude of 10 db above the shuttle design specification limit, falling below that limit above 10 KHz. The vehicle potential remained within the range of -3 to +1 volt throughout the flight which exhibits normal behavior for a satellite in a low equatorial orbit. The measured electron densities and temperatures are compared with the International Reference Ionosphere showing measured densities somewhat lower (up to a factor of 10) and temperatures higher (up to 400° K) than the reference model.

INTRODUCTION

The objective of this experiment is to characterize the electrical interaction of the shuttle with its environment. This report describes the experiment and its operation through a shuttle mission during which the instrument functioned normally and acquired 11.3 hours of data.

DESCRIPTION OF EXPERIMENT

The electric field experiment consists of a 1.575 meter dipole, illustrated schematically in Figure 1 as sensors A_1 and A_2 mounted along the orbiter X axis. These sensors are 2 1/4" diameter aluminum spheres mounted on 10" long booms on the equipment pallet which is mounted 16" above the trunnion fixture on the right hand (+ y) side of the cargo bay. This puts the sensors at a height of 22.5" above the edge of the cargo bay door 70" inboard. This geometry is such that when the shuttle attitude is right wing forward (+ y into velocity vector), then any

roll angle from -18.5° to + 158° will present the sensors with a clear view of positive ion flow.

The spheres are roughened to guarantee good adhesion and are coated with a graphite material, to ensure a uniform surface and constant work function. To obtain the electric field component along the dipole axis, the difference in potential between spheres A_1 and A_2 are measured with circuitry having a much higher input impedance than the resistance between the spheres through the plasma. This potential difference is input to Telemetry at two sensitivity levels, one a factor of five more sensitive than the other. In addition this potential difference is fed to two swept frequency receivers, sweeping simultaneously over the frequency ranges 0 to 66 KHz and 0 to 5 MHz in an eight second period. Details of the different measurements, sensitivies, sampling rates, etc., are given in Table 1. The amplifiers were calibrated by superimposing spikes, at known frequencies, on the signals for one eight second sweep 504 secs after instrument turn-on and at 520 second intervals thereafter. To obtain the required 5 MHz response it was necessary to situate pre-amplifiers as near the sensors as possible which resulted in this circuitry being located inside the sensor supporting booms attached directly to the sensor. Because it was critical that the temperature of these elements not exceed 60°C when operating, a temperature sensor was co-located with this circuitry in one of the booms (A_1) and was closely monitored during the mission.

In order to measure the state of charging of the vehicle with respect to the local plasma the potential of A_1 was also measured with respect to the spacecraft skin (ground), thus giving the spacecraft potential with respect to the plasma at the two points A_1 and A_2 (separated by 1 1/2 meters). Because almost the whole spacecraft is electrically isolated from the surrounding plasma by the thermal tiles, leaving the engine thruster nozzles as the only conducting surface by which the spacecraft potential can anchor itself to the plasma, it would be expected that the spacecraft potential would vary substantially. This was indeed found to be the case on STS-3 (ref. 1). In order to make vehicle potential variations of more than a few volts less likely, another experimenter (NRL-802) provided a "ground plane" of 1/3 square meter area mounted in the shuttle X Z plane approximately 70 cms in the -Y direction from the dipole axis, see Figure 1. This surface is connected to spacecraft ground and is effective in stabilizing the vehicle potential when the ion flow is normal to the surface, i.e., when the vehicle velocity vector is in the spacecraft +Y direction.

The second part of this experiment is the Electron Density sensor which is mounted midway between the electric field sensors (B, Figure 1) and offset inboard from the dipole axis by 10 cms. This sensor consists of a gridded sphere 2 1/4" in diameter with an open/surface ratio of 0.8 mounted concentric with a 1 3/4" diameter collector. The two elements are gold plated to reduce work function potential differences between the surfaces. The inner sphere is biased at +20 volts with respect to the outer sphere, which voltage is sufficient to collect all electrons of energies below 30.625 eV which enter the outer grid and to reject all ions with energies below 20 eV, that is all ions below mass 65AMU moving with the ram velocity (7.7 Km sec^{-1}) which includes the dominant ionospheric ions. Thus, the sensor filters out, and collects the current due to only electrons, which is then input to a logarithmic electrometer measuring in the current range 10^{-9} through 10^{-4} amps. The output is fed to telemetry and to an A.C. amplifier with a gain of 40, then through a bank of eight filters to telemetry giving outputs which measure the electron density irregularities $\Delta N/N$.

The potential on the outer grid of the sensor with respect to ground is programmed to operate 50% of the time as a Langmuir probe where the voltage is varied linearly as a function of time, and 50% in a Irregularity measurement mode where the voltage is kept constant. This programming is depicted in the lower part of Figure 2 where the upper part shows in a block format the signal processing system. To obtain density, temperature and vehicle potential from the Langmuir probe operation it is necessary that the probe be swept through the local plasma potential. To allow for the possibility of the vehicle potential being anywhere in the range of -20 to +4 volts, the + 4 volt sweep was applied with respect to a bias voltage which was stepped at $\frac{1}{64}$ sec intervals through 0, +4, +8 and +16 volts.

This operation was controlled with an internal timer, synchronized to the telemetry frame rate through a 100 Hz clock, and recycled every 256 secs when a timer reset pulse was transmitted to telemetry.

EXPERIMENT PERFORMANCE

Table 2 summarizes the vehicle history and the amount of data acquired in each vehicle attitude. The experiment was commanded on and off by command sequences that were capable of operating for roughly 24 hours before they required updating. This system worked quite well but had the disadvantage that last minute changes in the astronauts schedule caused planned events to be missed. For example, it was important to obtain background EMI data with the payload bay doors closed, thus shutting out the environmental noise. This event was missed completely because of difficulties encountered on the first closure attempt.

Much of the data was acquired in 5 minute "snapshots", longer operating periods were more desirable of course, and were obtained mostly in the gravity gradient and bay-to-earth attitudes. The two longest periods were of 45 minute duration in the bay-to-earth attitude.

In Figure 3a and 3b are shown the temperatures of the electronics package (A452) and the E-field sensor boom A1 (T808) respectively, on 3a is also indicated the vehicle attitude. The payload by doors were opened at Mission Elapsed Time (MET) = 7,305 secs which was 94 minutes prior to the first data acquisition at Revolution (Orbit) number 3.6 when the electronics package and boom were at approximately room temperature of 20°C. Thereafter the electronics cooled to near zero by REV #9.5 where it remained for the rest of the mission. The excursions up to 11°C and 17°C can be seen to coincide with the two Bay-to-Sun (- ZSI) periods. In general, the electronics package temperature increased, as expected, as a function of "on" time except from MET = 170,000 through 200,000 where the pallet was cooling faster than the electronics warmed up. On the other hand, in Figure 3b, the booms being thermally isolated from the pallet experienced wider temperature oscillations ranging from + 30°C in Bay-to-Sun periods down to -40°C at night when the cargo bay faced away from the earth. Thus, the temperature seen on the booms depends solely on the sun/shadow situations.

EXPERIMENT RESULTS

Vehicle charging for the entire mission will be discussed, then typical AC electric field values will be compared to shuttle specifications for broadband emissions. Finally, electron densities and temperatures for a 45 minute period will be compared to an ionospheric model.

Vehicle Charging

Figure 4 shows the result of plotting 64 second averages of vehicle potential for almost all (the period from MET = 13,000 through 90,000 secs was accidently omitted) the periods when the instrument was operational during the mission. It can be seen that the general level in between -3 and +1 volts, which values are tyical for a satellite in a low equatorial orbit where the average electron energy is of the order of 0.16 eV.

Comparing figure 4 with the vehicle attitudes shown on Figure 3a it can be readily seen that the high value of +1.0 volts at MET ≈ 163,000 secs coincides with the bay-to-sun attitude (-ZSI) where photo-electron emissions from the instrument pallet (but not the reference plane, which is edge-on to the sun) drives the vehicle positive with respect to the reference plane. The three data sets near MET = 260,000 secs, where the vehicle potential approaches -4 volts were taken in a bottom-to-sun attitude (+ ZSI) during night-time conditions.

The more extreme variations, seen on the lower panel of Figure 4 (MET > 310,000 secs) ranging from -3.2 volts to + 1.8 volts were all taken during tail-to-sun attitude (- XSI). The positive values around MET = 317,000 secs and at MET = 352,000 secs are identified with the tail pointing into the velocity vector where the ram ion flow coupled with with a low photo-electron emission produces a net positive charge. The low potentials on the other hand, e.g., near MET = 440,000 secs, are identified with periods when the sensors and cargo bay are in the ion flow wake region.

Broad Band EMI

In Figure 5 we show a typical electric field power spectrum showing the amplitude in db μV/m MHz as a function of frequency on a logarithmic scale. The data from the low frequency sweep (0 - 60 KHz) is represented by squares and that from the high frequency sweep (0 - 5 MHz) as triangles, the lower limits for these measurements are 122 db and 107 db respectively. Shown also on this figure are the maximum shuttle-produced broad band noise limit (Design spec max) and the payload design specification, this latter is a specification for payload design whose limit is only given above 10 KHz whereas the former is based on ground shuttle measurements made by SAIL. It can be seen that below 10 KHz the measured broadband noise exceeds the design limit by a maximum of 12db in the frequency range of 1 to 2 KHz. This is due to electrostatic waves produced by the shuttle body moving through the environment. Taking the ambient oxygen temperature to be 1000° K gives a most probable oxygen speed (random thermal speed) of 1.019 Km/sec, thus a vehicle Mach Number of 7.5.

Other features to note on this figure are the line emissions at 37.5 KHz and the noise enhancements in the frequency range of 200 KHz to 5 MHz. The former is probably due to a DC/DC converter on the pallet which line was also seen on ground integration tests, the latter are probably genuine plasma emissions

since they occur in the frequency range of the plasma frequency (900 KHz - 9 MHz) and the electron gyro frequency (840 KHz).

Model Comparison

Comparison of measured electron densities and electron temperature with the International Reference Ionosphere (IRI) are shown in Figure 6 comprising of some 45 minutes of data taken on Rev #24.6. The IRI model is shown as solid lines and the measured data as points with vertical error bars. These data result from analysis of the Langmuir probe mode of operation of the electrons sensor where each 8 second interval results in two points, one from the upsweep (-4 to +4 volts) and one four seconds later from the downsweep (+4 to -4 volts). Because of a well-known hysteresis effect, where electrons accumulate on the outer grid giving an effective grid potential offset from the applied potential, the deduced densities and temperatures differ slightly. In each successive 256 second period only the first 128 seconds gave usable Langmuir probe data, the +8 and +16 volt biases applied at 128 and 196 seconds, respectively produced near-saturation currents.

Comparing the model and measured densities in Figure 6a it is seen that the measured values are lower by up to a factor of 10. On the other hand, the measured temperatures in Figure 6b are in general higher than the model. These differences are explained by the fact that the electron sensor is located in the cargo bay, hence, embedded in the vehicle sheath. If the balance of the sheath has only a net negative charge with respect to the ambient plasma of only a few hundreths of a volt, then a fraction of the lowest energy ambient electrons will be unable to reach the sensor location thus giving the low observed densities and high observed temperatures.

VEHICLE INDUCED EFFECTS

The following three sections describe the effects of a main engine burn, vernier thruster firings and a water dump.

OMS-4 Burn

Figure 7 represent data taken during the fourth burn of the OMS motor, ignition occurred at MET = 18,852.4 secs for a 30 sec burn durations. On the time scale of Figure 7a the burn starts at 169 seconds and ends at 199 seconds. On the upper panel is shown the plasma potential with respect to the vehicle that is, the potential of the Al sensor on a scale of -9 to +9 volts. The vehicle potential (with respect to the plasma) is the measured quantity with reversed sign thus it can be seen that prior to 170 seconds the vehicle potential is -0.7 volts. The second panel shows the potential difference between the electric field sensors on a scale of -2 to +2 volts, and the third panel is the same quantity on a ten times larger scale. The electric field is obtained by dividing this voltage by 1.575 (dipole separation distance in meters) and gives the component in the -x (nose-to-tail) direction. Thus, it can be seen that the electric field varies from 160 mV/m at time 0 seconds to zero at 256 seconds. A small electric field component along the Shuttle X-axis is expected here because the vehicle is flying in an "aeroplane" attitude (zero pitch and zero yaw) to increase the orbital altitude during the motor burn. The dominant

electric field is due to the vehicle motion through the geomagnetic field, $V \times B$, contributing no field component along the velocity vector in this vehicle attitude.

The lower panel shows on a logarithmic scale the current measured by the electron sensor ranging from 10^{-9} amps to 10^{-3} amps. In section 2 it was pointed out that a bias potential was applied to the sensor with respect to the vehicle and stepped at 64 second intervals through 0, 4, 8 and 16 volts. The effect of this can clearly be seen on this panel where only the constant voltage mode data are shown occurring at even 8 second intervals.

In the time period up to 64 seconds the current is very low where the electrons are being retarded, at 64 seconds when the bias is stepped from zero to +4 volts the current increases over four orders of magnitude because we have now shifted to a voltage where the electrons are accelerated to the sensor. Reading the vehicle potential from the top panel as - 0.7 volts it can be seen that we have moved the sensor potential from - 0.7 volts to + 3.3 volts with respect to the plasma at 64 seconds. At 128 seconds the sensor potential is stepped up another 4 volts to + 7.3 volts with respect to the plasma and the amplifier saturation current of 1.363×10^{-4} amps is almost reached. The final step to 16 volts bias at 196 seconds now saturates the amplifier.

Turning now to the effects of the motor burn. At motor ignition the vehicle potential initially swings negative by almost 2 volts (A1 increases) at 169 seconds, returns to its pre-ignition value of - 0.7 volts in 0.2 seconds and then decreases linearly through the 30 second burn period to - 1.0 volt at 199 seconds. This vehicle potential fluctuation is consistent in sign with the electron current observed on the lower panel in Figure 7a and on an expanded time scale on the lower panel of Figure 7b, where the negative excursion of sensor potential causes a current reduction of 3 orders of magnitude, i.e., apparently takes the sensor potential to zero or slightly below plasma potential. Since the sensor potential prior to motor ignition is + 7.3 volts an excursion of some - 7.5 volts would be necessary to reduce the sensor current to the observed 10^{-7} amps. An alternative explanation is that motor ignition causes a sudden increase in pressure in the local environment which changes the electrical vehicle sheath condition. This hiatus interrupts the flow of electrons to the sensor and could also possibly explain the apparent positive excursion of vehicle potential, seen as a negative excursion of approximately 1.5 volts on A1 at 169 seconds.

Looking at the electric field response on Figure 7a, A1-A2, we see no change in the D.C. electric field but a very apparent increase in noise from 0.2 volts to 0.5 volts peak to peak amplitude throughout the 30 second burn period. This increase in "noise" can be seen by comparing the upper two panels in Figures 7b and 7c, where the spectra are shown for two succesive frequency scans 7c before motor ignition and 7b during and following ignition. Ignition occurs at 1.2 seconds on 7b the vertical scale is proportional to the log of E^2 measured in v^2/m^2Hz and the spectra show the receiver frequency being swept linearly as a function of time. Comparing the amplitude at 5 KHz on either side of the 0 KHz pedestal it is seen that ignition produces a noise value an order of magnitude higher than the subsequent burn noise, which is again an order of magnitude higher than the noise prior to burn. By comparing the 0 KHz peaks it is seen that this noise is at a low ($<$ 1 KHz) frequency. Again, a probable explanation for this increased electrostatic noise is a large local pressure increase, with the additional possibility that the electrostatic noise and the $\Delta N/N$ enhancements are due to the propagation of a sound wave through the plasma.

Thruster Firings

Of the 44 thrusters that make up the Reaction Control System (RCS), 38 are primary (PRCS) and six are vernier thrusters (VRCS). This latter system is the one employed for attitude control for the major part of this mission and are the ones which we will discuss. Two are situated in the nose and four, two left and two right, on the engine pod just above the trailing edges of the wings. Of these six vernier thrusters those in front produced no discernable effects, those on the left small perturbations and those on the right large effects with the thruster firing down producing larger fluctuations than the one thrusting to the right. The reason for this difference is probably that the right aileron could, if left in a horizontal position deflect part of the thruster plume upwards towards the starboard cargo bay area where the instruments were located.

The thruster firing effects are shown in Figure 8 with a time history of firings shown in table 3. During this acquisiton period the vehicle was in a bay-to-sun attitude with the right wing (+Y) pointing into the velocity vector (approximately eastward). The local time is near midnight thus the cargo bay is facing the earth and again the measured component of the $\overline{V} \times \overline{B}$ electric field is small (A1 - A2), on Figure 8a. The total thruster firing period of 12.88 seconds commencing at 184.58 seconds is shown in the upper panel of Figures 8a, b, and c. It can be seen that the effects are barely discernible on either vehicle potential (A1) or D.C. electric field (A1 - A2),. but produce a factor of ten decrease in the electron current. This current response cuts off at 192 seconds due to the sensor switching into the Langmuir probe mode of operation, we will return to this later.

The outputs from the eight $\Delta N/N$ filters are shown in Figures 8b and 8c on the same time scale as 8a with again the thruster firing indicator in the top panel. The vertical scale is logarithmic extending from -0.1 to +4.9 with 0 being equivalent to 0% value of $\Delta N/N$ and 5 corresponding to 186% $\Delta N/N$. The large oscillations up to 64 seconds, the smaller oscillations up to 128 seconds and the large negative going vertical spikes thereafter are due to switching in and out of the Langmuir probe mode of operation. An explanation of the positive spikes discernible on all the filter outputs at a time interval of 5 seconds, which come and go throughout the mission has not been found. It is perhaps a cycling time of another experiment or a payload switching operation, this is being investigated. The general signal level is the quantity to note. It can also be seen that the signal level is depressed for frequencies greater than 100 Hz in the first 64 seconds. This is due to the roll-off in frequency response of the logarithmic amplifier above 100 Hz at the lowest current level of 10^{-9} amps, which is the current level indicated on the lower panel of Figure 8 a. The thruster firing effect can be seen starting at 184.6 seconds and extending through 194 seconds, coinciding exactly with the right thruster firing times listed in table 4. No effects are discernible either from the front left firings nor at termination of the front right operation at 197.5 seconds. The right thruster produces an increase in $\Delta N/N$ from 0.5% to 1.6% at 30 Hz, decreasing to zero effect at 500 Hz where $\Delta N/N$ = 1.6%, changing to a suppression with increasing frequency to a maximum of a depression in $\Delta N/N$ from 5% to 0.5%.

An even more dramatic effect of the decrease in noise due to thruster operation can be seen in the Figure 8d through 8g which shows a series of four consecutive spectra from the A.C. electric field outputs. The panel format is the same as in Figure 8 (b and c). These figures show in the third panel the current decrease

at the firing start in 8e at 0.2 seconds and then return to its initial value at 1.7 seconds in 8f coincident with the right thruster firing end. Note the almost complete suppression of all frequencies greater than 12 KHz in the top two panels of Figure 8e as compared with 8d, f or g, the reduction in electrostatic noise above 3 KHz and the small increase at frequencies below 2 KHz. These effects are very similar to those observed by the Plasma Diagnostic Package[1] on STS-3, and offer a possible explanation in terms of a local pressure increase caused by gases emitted from the starboard thruster.

Water Dump

A water dump occurred on Rev #33.6 commencing at MET = 175864.84 seconds the effects of which are shown in Figure 9. At this time the vehicle was in a tail-to-sun attitude and was just crossing the terminator from day to night which puts the shuttle in an "aeroplane" attitude with the cargo bay facing away from the earth and the electric field dipole aligned with the velocity vector hence a zero $\bar{V} \times \bar{B}$ electric field component.

The water dump start is shown in the upper panel of Figure 9a at 181.4 seconds and continuing through 256 seconds. The vehicle potential decreases by a very small amount -0.2 volts (A1 increases), the D.C. electric field (A1-A2) remains unchanged but the noise increases from 0.1 volts peak to peak to 0.15 volts and the electron density which has been steadily decreasing, increases at the start of the dump by some 10% but sustains the same rate of decrease during the water dump as before.

Looking at the $\Delta N/N$ data in Figures 9b and 9c we see a progressive enhancement of $\Delta N/N$ from 30 Hz up to 503 Hz during the water dump which then decreases back to zero effect at the highest frequency of 7.830 KHz. Figures 9d and 9e show the electrostatic frequency spectra before and after the water dump start the only difference to be noted in the slight filling in around 0 KHz on the low frequency spectrum on 9e compared to 9d. This indicates that the increase in noise on (A1-A2) in Figure 9a occurs at frequencies less than 2 KHz. The explanation for these measurements is probably the presence of eater droplets charged by triboelectric effects and a local increase in pressure.

CONCLUSIONS

1. There exist electrostatic noise at frequencies below 10 KHz generated by body motion at about 135 db V/m MHz amplitude which propagate to the sensor location in the cargo bay.

2. At OMS ignition a large pressure wave is generated for 3/10 second which shields the cargo bay area from the environment.

3. The OMS burn and thruster firings produce acoustic noise detected by its electric field and $\Delta N/N$ effects in addition the local pressure increase produced by starboard thruster reduce the electron density by a factor of 10.

4. Ambient plasma measurements of electron density, irregularities, temperature and electrostatic waves are possible in the cargo bay provided that the shuttle attitude is correct and that appropriate exposure factor corrections are made.

5. Measured vehicle potentials were typical of a satellite in low earth orbit ranging in value from -3 to +1 volts with typical values of around -1 volt.

REFERENCE

1. Shawhan and Murphy, "Plasma Diagnostics Package Assessment of the STS-3 Orbiter Enviornment and Systems for Science", (1982).

TABLE I INSTRUMENTATION AND MEASUREMENTS

1. Electric Field Sensor

DIPOLE LENGTH = 1.575 meters

Measurement	Range	Sensitivity	Sample Rate
a) Probe Potential (AI)	-8.156 to +8.494 volts	± 33 mV	25/sec
b) E-Field LO (DC)	-1.059 to +1.104 V/m	± 7 mV/m	25/sec
c) E-Field HI (DC)	-1061 to -628 mV/m	± 1mV/m	25/sec
d) E-Field LO (AC)	0 to 66 KHz 209 Hz/sample	To $10^{-11.587}$ to $10^{-4.196} v^2/m^2/Hz$	50/sec
e) E-Field HI	0 to 4.991 MHz 14.680 KHz/sample	$10^{-14.664}$ to $10^{-7.678} v^2/m^2/Hz$	50/sec

2. Electron Density Sensor

COLLECTION AREA = 1.026×10^{-2} m^2

Measurement	Range	Sensitivity	Sample Rate
a) Electron Density	15 to 2 x 10^6 cm^{-3}	± 2%	25/sec
b) Electron Temperature	100 to 100,000°K	± 2%	
c) Vehicle Potential	-20 to +4 v	± 80mV	
d) ΔN/N	0 to 186% 30, 60, 115, 503, 968, 1939, 3900 AND 7830 Hz	± 0.05%	10/sec (each filter)

3. Housekeeping

a.	Electronics Package Temperature	-80°C to 150°C
b.	Boom AI Temperature	-80°C to 150°C
c.	Timer Reset Indicator	1 sample/sec

TABLE 2

REV # from	REV # to	Mission Elapsed Time (Secs) from	Mission Elapsed Time (Secs) to	Vehicle Attitudet	Data Acquired (Mins)
3	3	12,952	13,552	-ZLV, XPOP, 12° roll	10.0
4	4	18,683	18,983	OMS-4 Burn	5.0
5	6	22,787	29,864	GG	28.167
8	12	36,900	60,068	+ZSI	23.333
13	16	65,158	85,025	-ZSI	40.0
18	21	92,454	109,781	GG	93.333
22	29	113,182	152,527	-ZLV, XPOP, 12° roll	110.0
29	32	154,504	170,063	-ZSI (IECM*)	55.0
33	37	174,052	197,215	-XSI (IECM*)	47.0
38	52	202,171	279,577	+ZSI	142.333
54	59	313,450	313,750	PTC	5.0
59	94	317,084	506,268	-XSI	147.9
				TOTAL	677.066 = 11.284hrs

* This is the period over which the NASA Induced environment contamination monitor was operating.

† Description of attitude terms:

-ZLV, XPOP, 12° roll = bay (-Z) to earth, X perpendicular to orbital plane, 12° roll cants right wing out of velocity vector.
GG = gravity gradient, approximately nose to earth, right wing into velocity vector such that a stable attitude is achieved.
+ZSI = Bottom to sun
-ZSI = Top (Cargo bay) to Sun
-XSI = tail to Sun
PTC = "Rotisserie" mode, X perpendicular to earth-sun line with a slow roll

TABLE 3. - THRUSTER OPERATION

Thruster	Start (MET) secs	Stop (MET) secs	Start (Fig 7) secs	Stop (Fig 7) secs
FRONT RIGHT	274633.38	274646.26	184.58	197.46
RIGHT RIGHT	274633.38	274642.74	184.58	193.94
FRONT LEFT	274633.38	274634.34	184.58	185.54
FRONT LEFT	274636.26	274636.74	187.46	187.94
FRONT LEFT	274638.66	274639.14	189.86	190.34
FRONT LEFT	274641.06	274641.54	192.26	192.74
FRONT LEFT	274642.74	274646.26	193.94	197.46

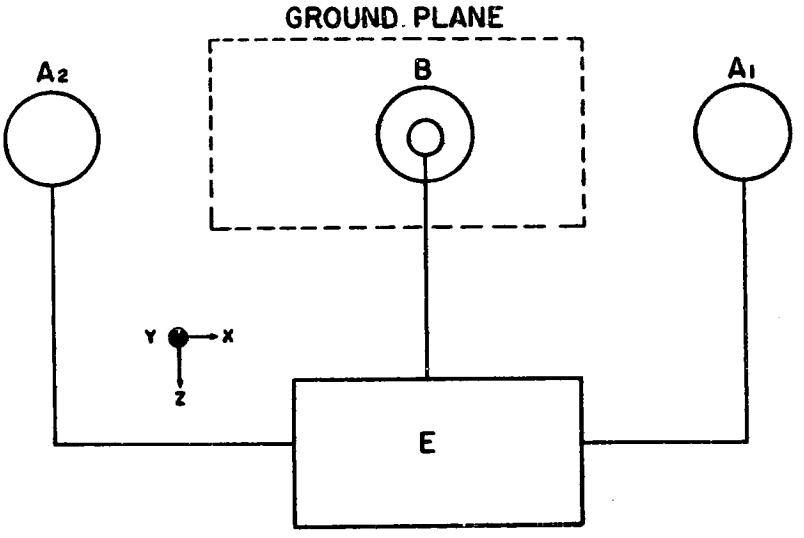

Figure 1. - Schematic layout of electric field dipole (A_1, A_2) and electron sensor (B) with shuttle coordinate area.

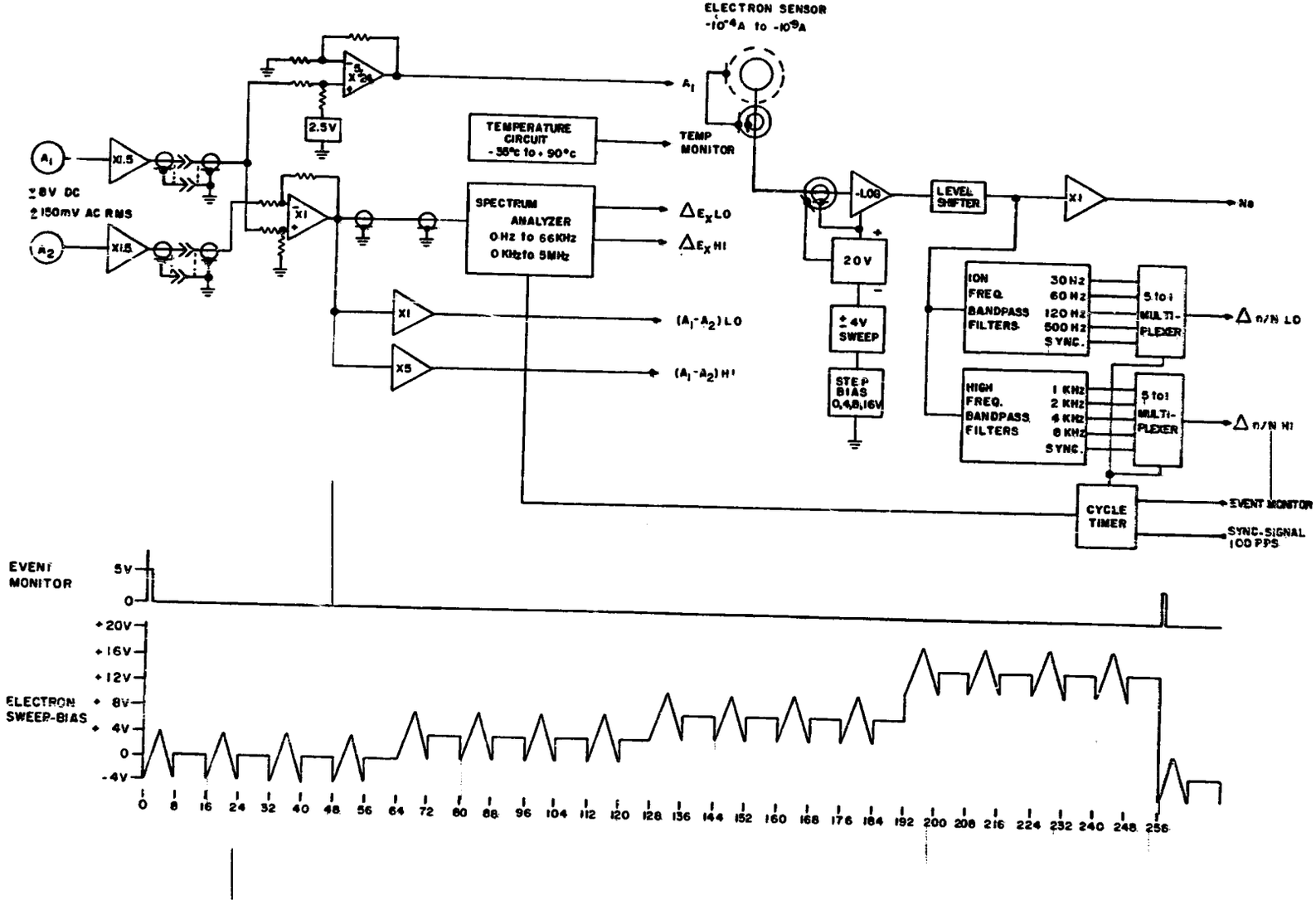

Figure 2. - Signal processing system and electron sensor voltage program.

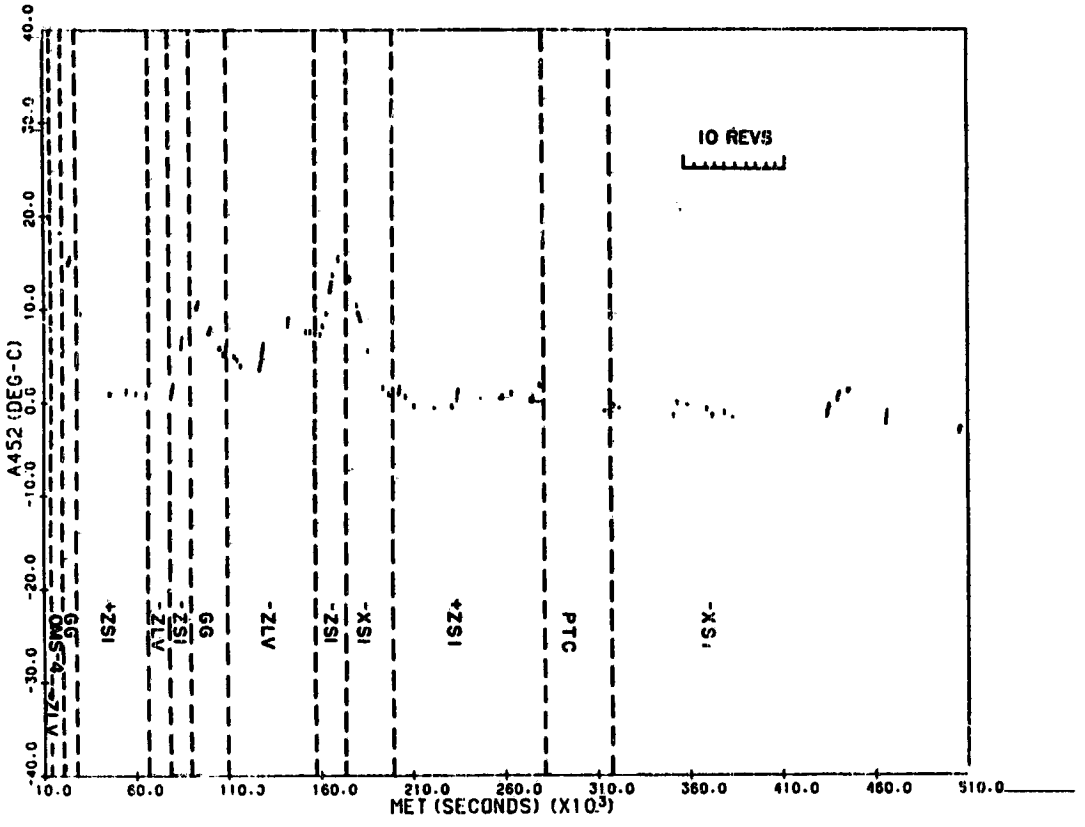

(a) 804C temperature A452.

Figure 3. - Electronics unit temperature (A452) with vehicle attitude and boom A_1 temperature (A808) versus mission elapsed time.

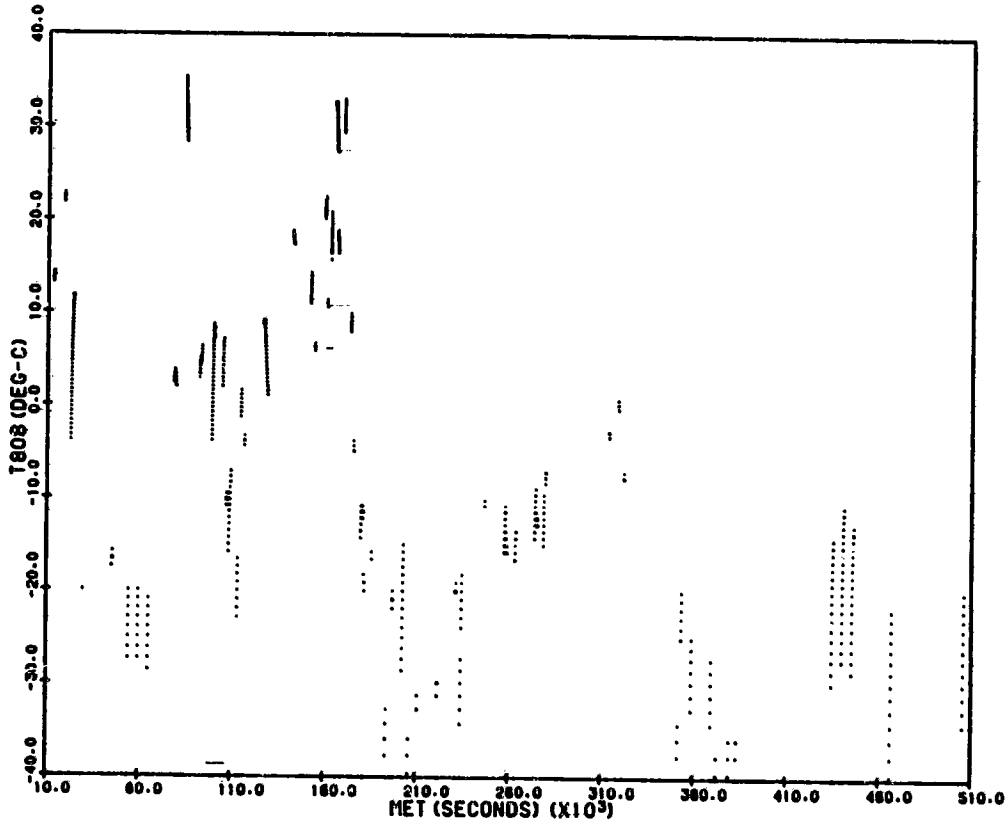

(b) 804C temperature T808.

Figure 3. - Concluded.

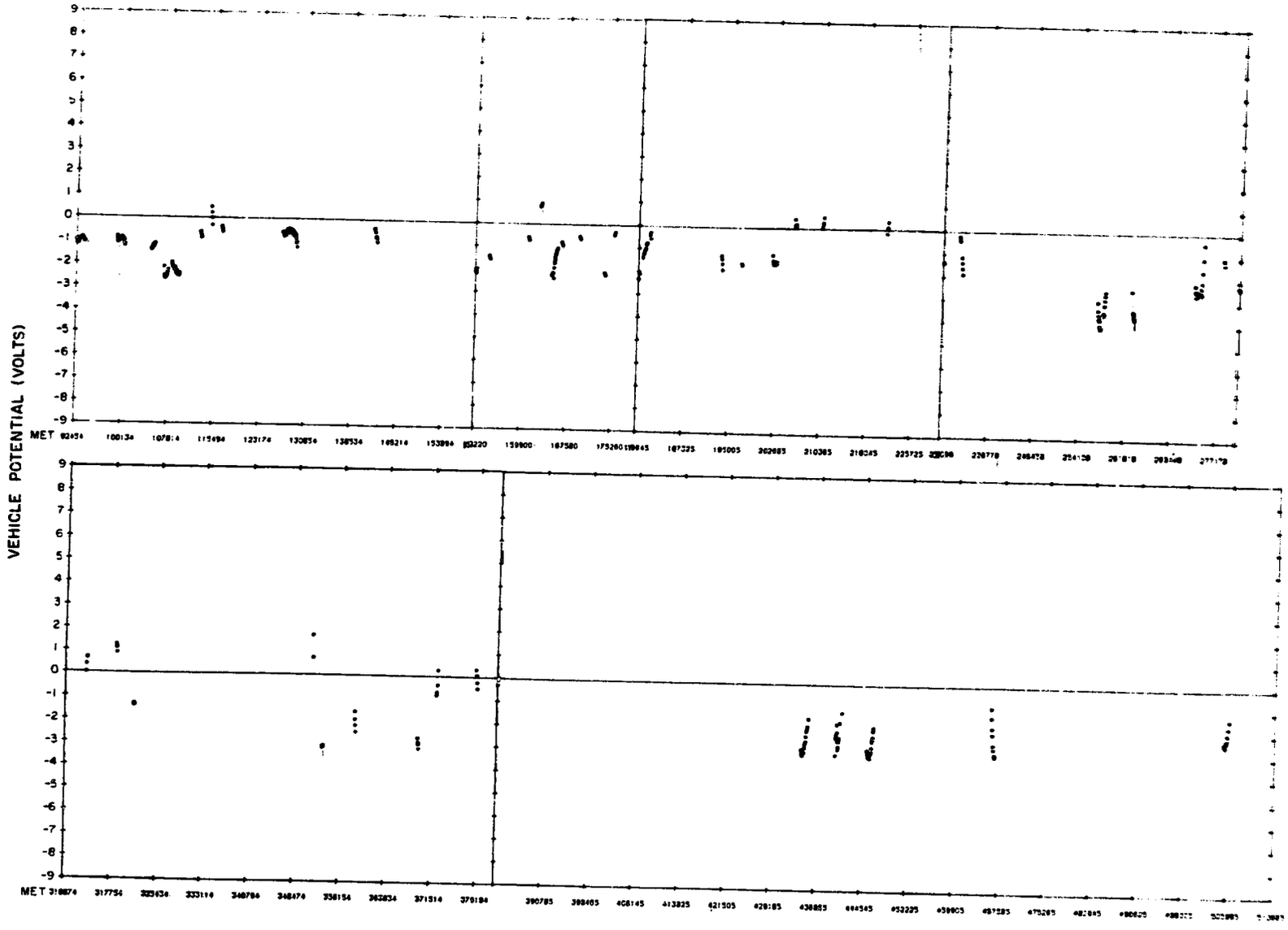

Figure 4. - Vehicle potential for all data collection periods for orbit 18.2 (MET = 92 454 sec) through orbit 94.3 (MET = 505 362 sec).

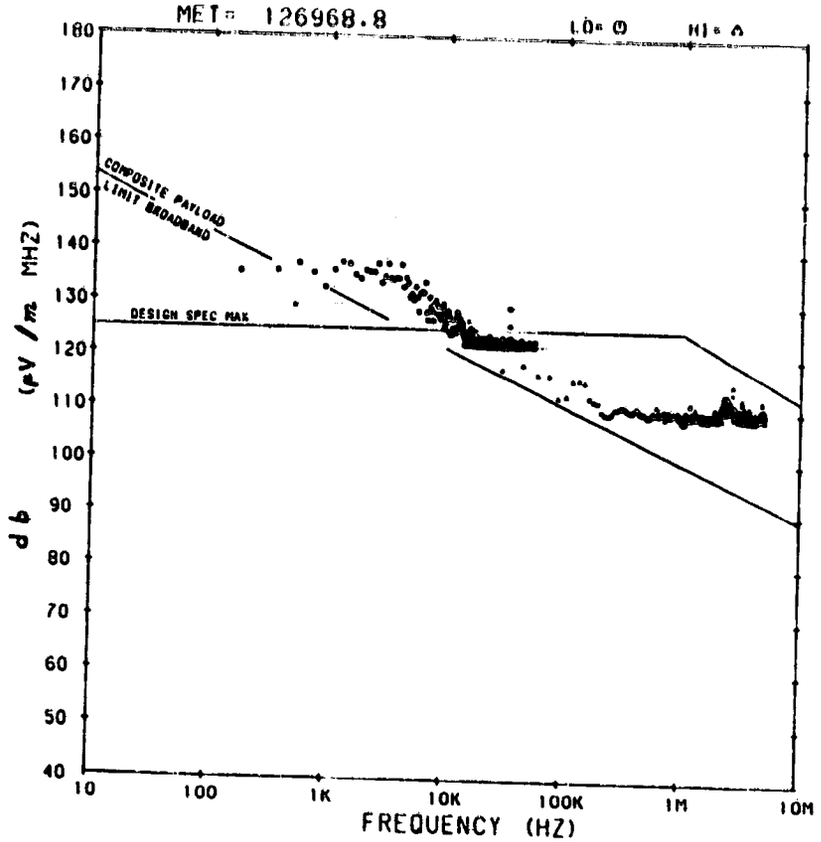

Figure 5. - Typical power spectrum of electrostatic noise.

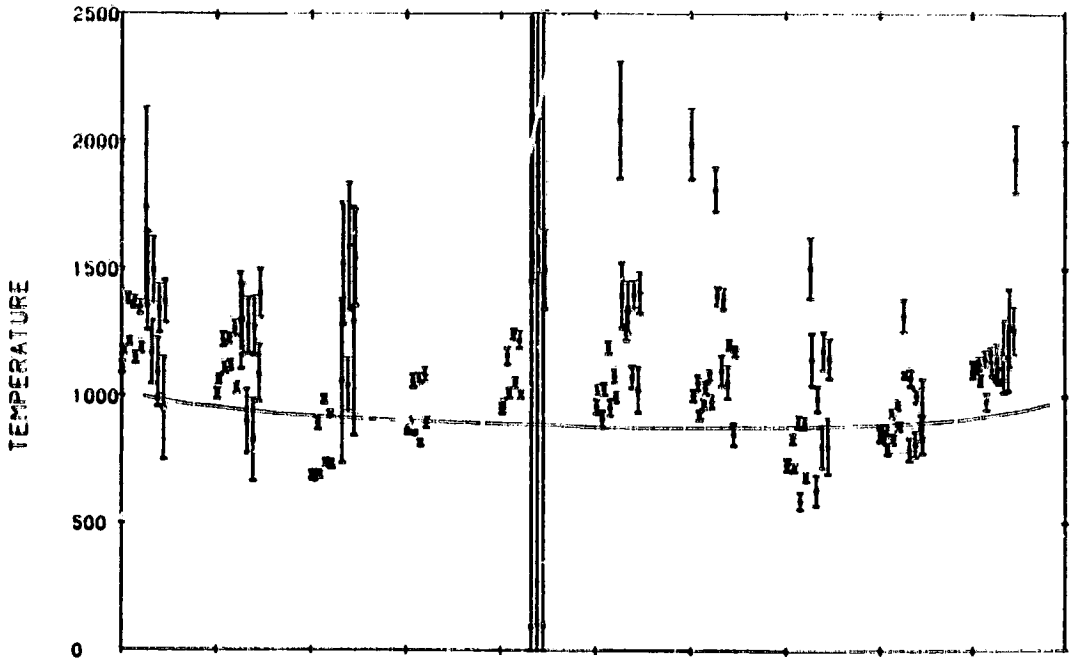

(a) Electron density.

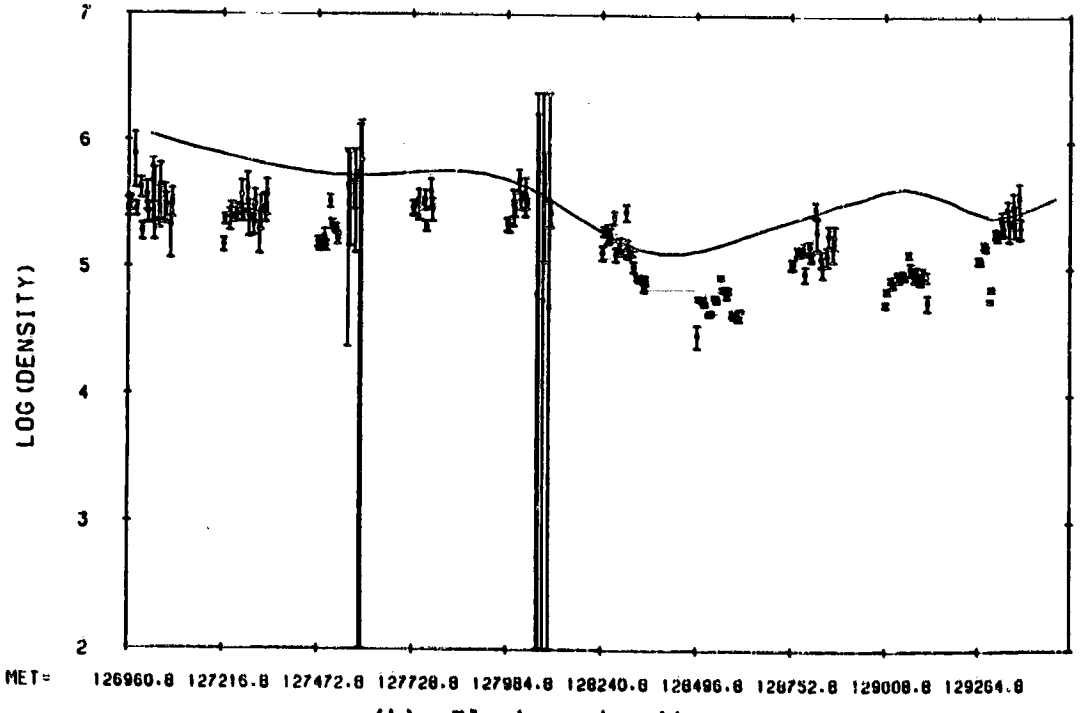

(b) Electron density.

Figure 6. - Comparison of electron density and electron temperature (points with error bars) against International Reference Ionospheric model (solid line) versus time.

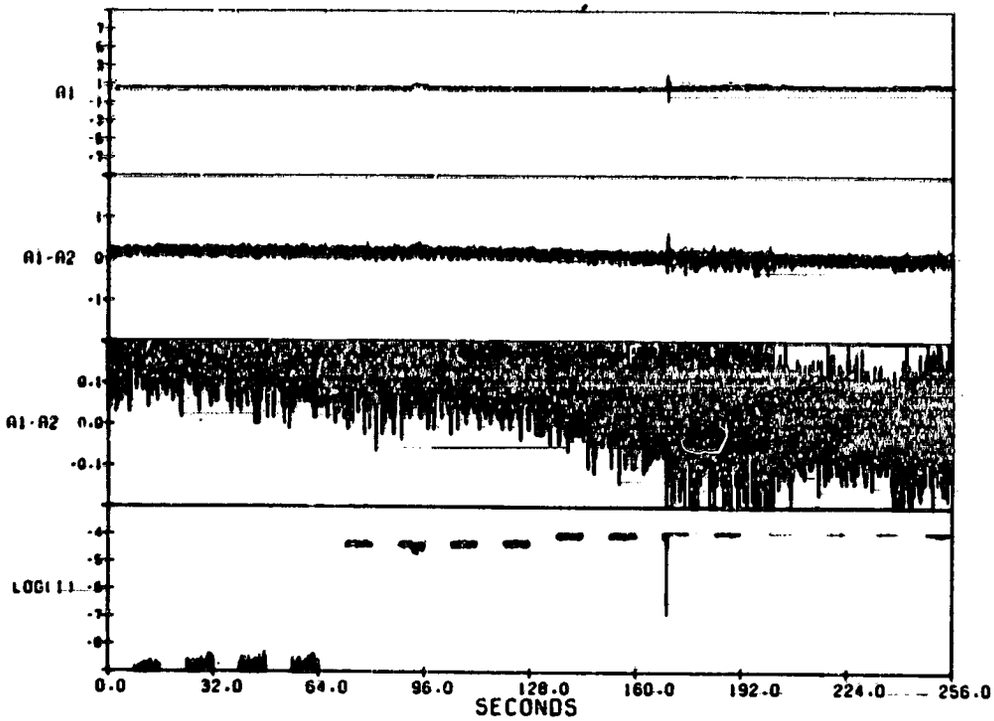

(a) Vehicle potential, electric field, and electron current versus time MET 18 683.4 sec.

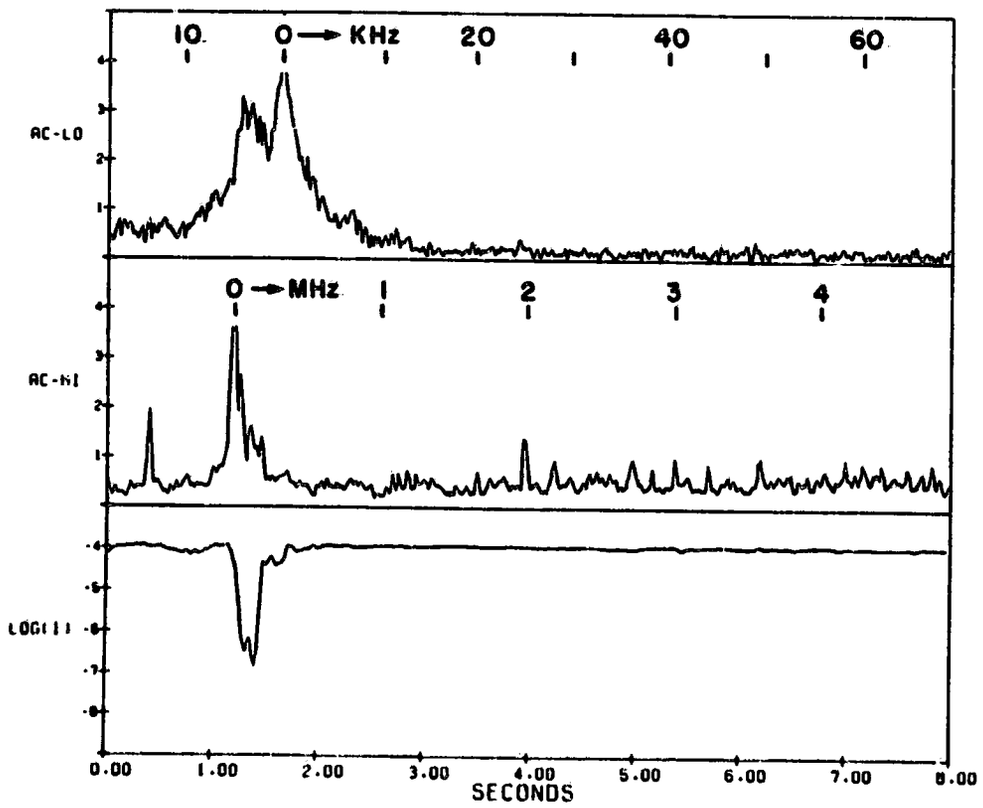

(b) Electrosatic spectr over low- and high-frequency ranges and electron current versus time. MET, 18 851.4 sec; inteval 22.

Figure 7. - OMS-4 burn.

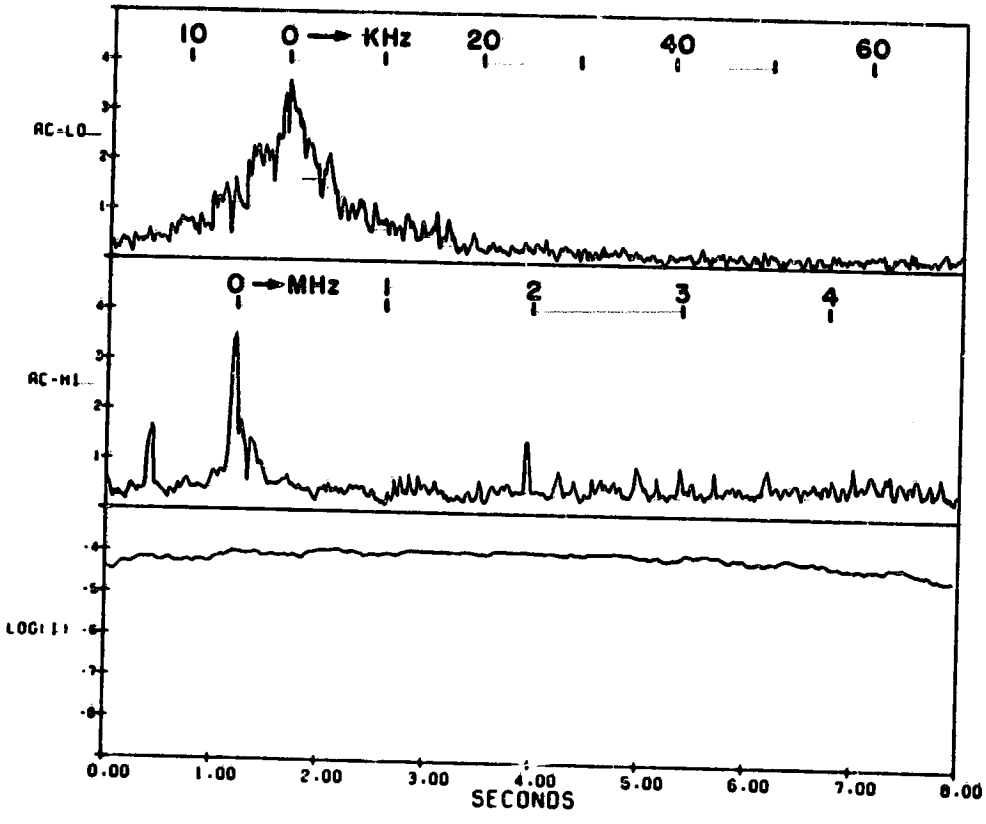

(c) Electrostatic spectra over low- and high-frequency ranges and electron current versus time. MET, 18 843.4 sec; interval 21.

Figure 7. - Concluded.

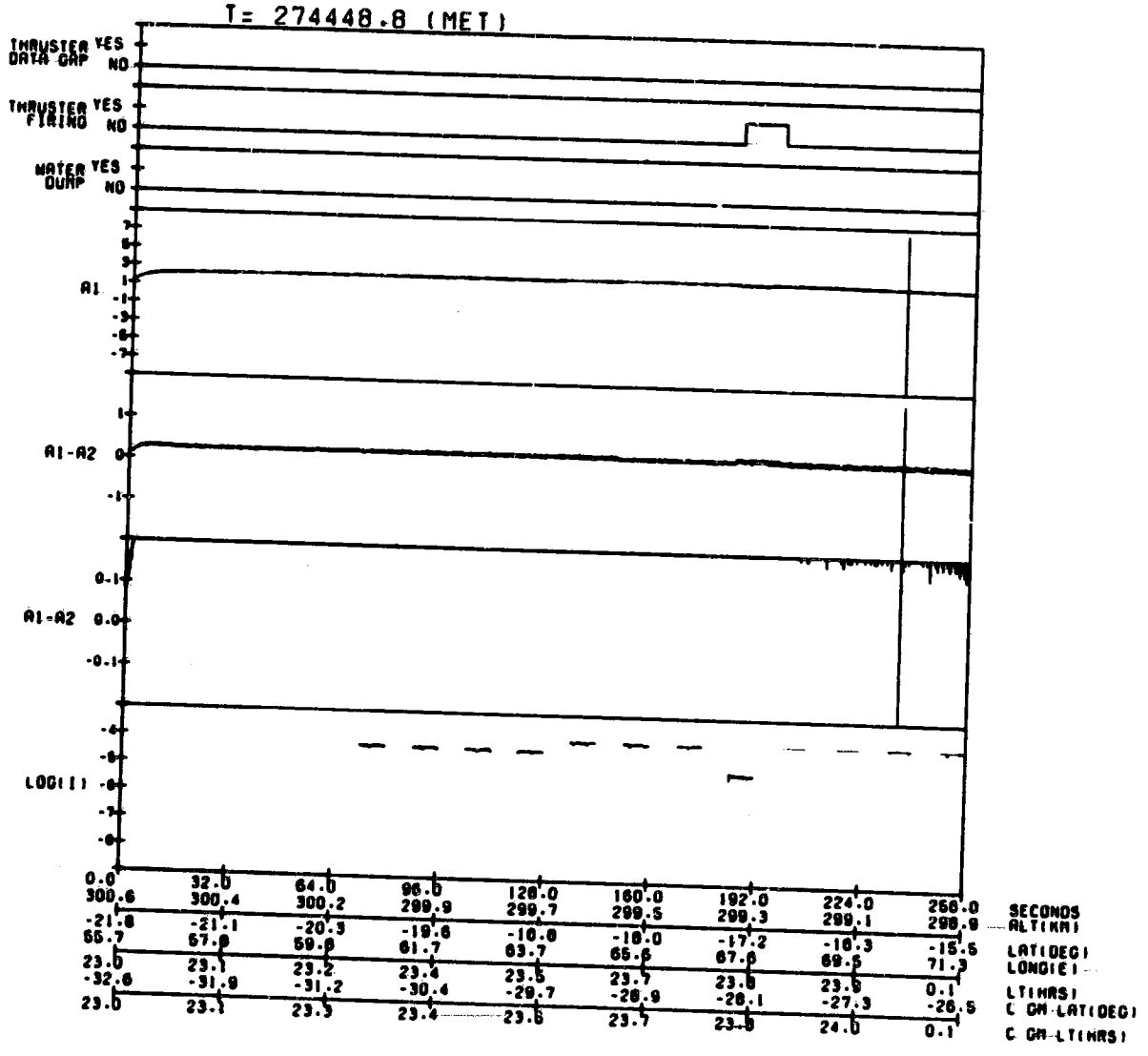

(a) Thruster firing indicator, vehicle potential, electric field and electron current versus time and orbital position.

Figure 8. - VRCS firings.

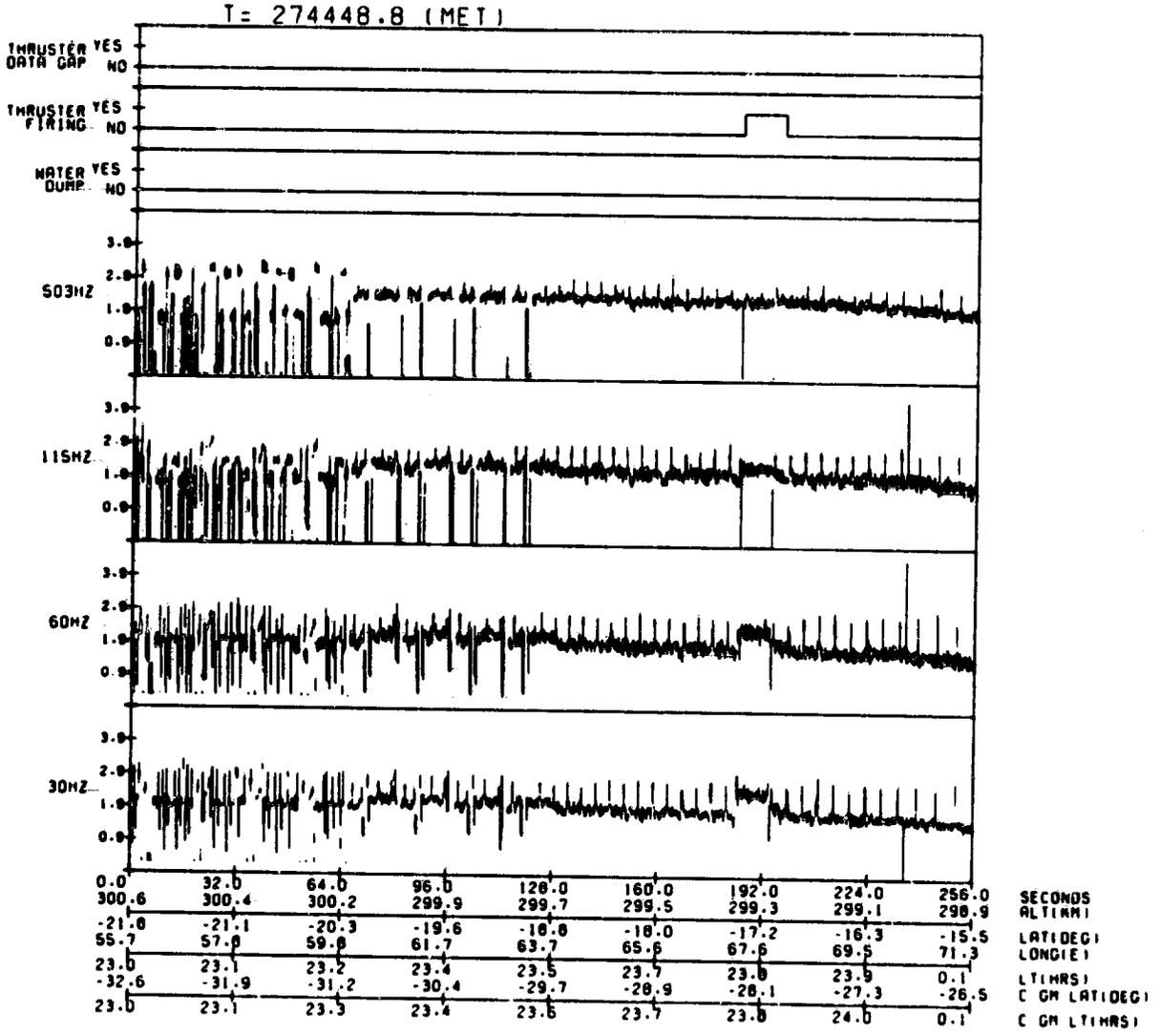

(b) Thruster indicator ΔN/N filter outputs versus time and orbital position.

Figure 8. - Continued.

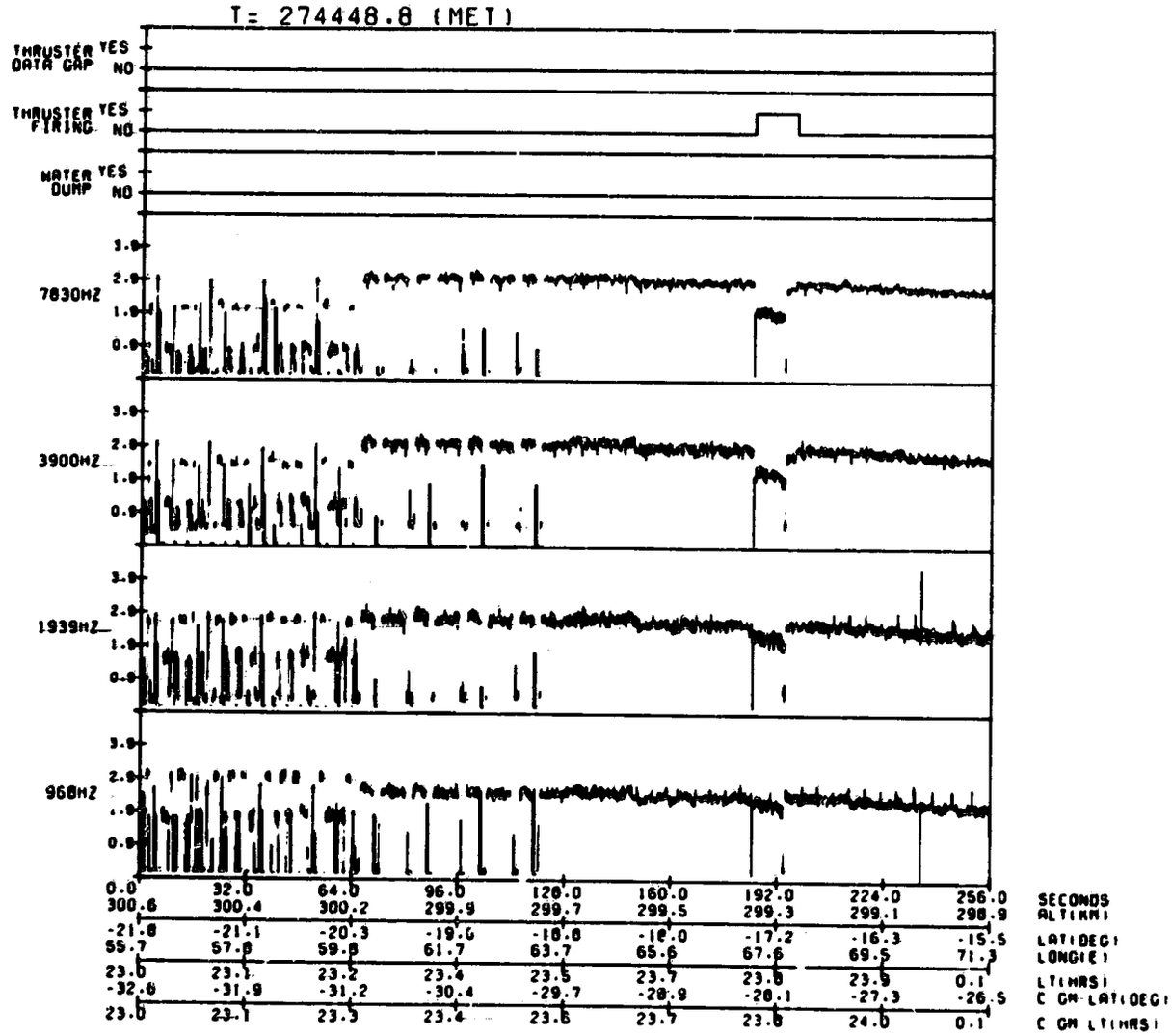

(c) Thruster indicator ΔN/N filter outputs versus time and orbital position.

Figure 8. - Continued.

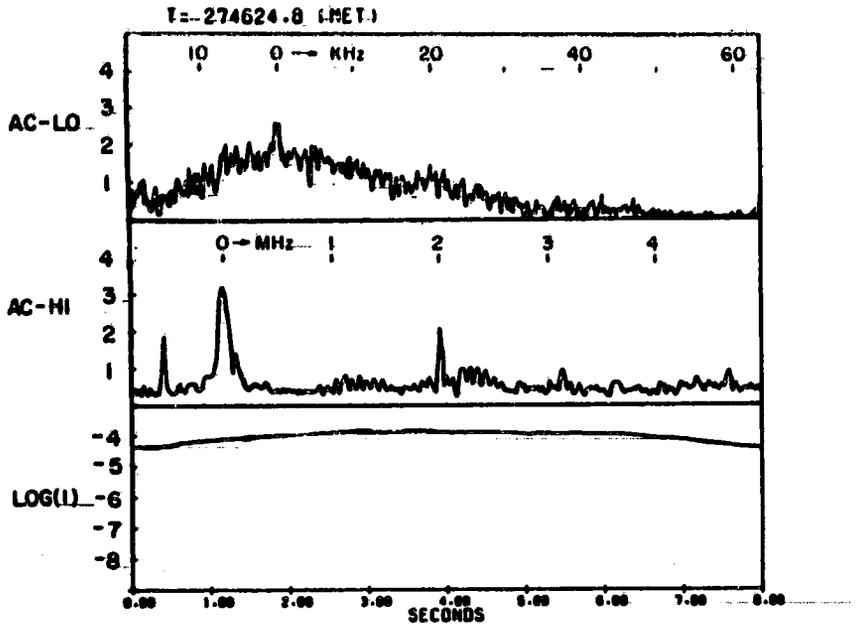

(d) Electrostatic spectra over low- and high-frequency ranges and electron current versus time. Interval 23.

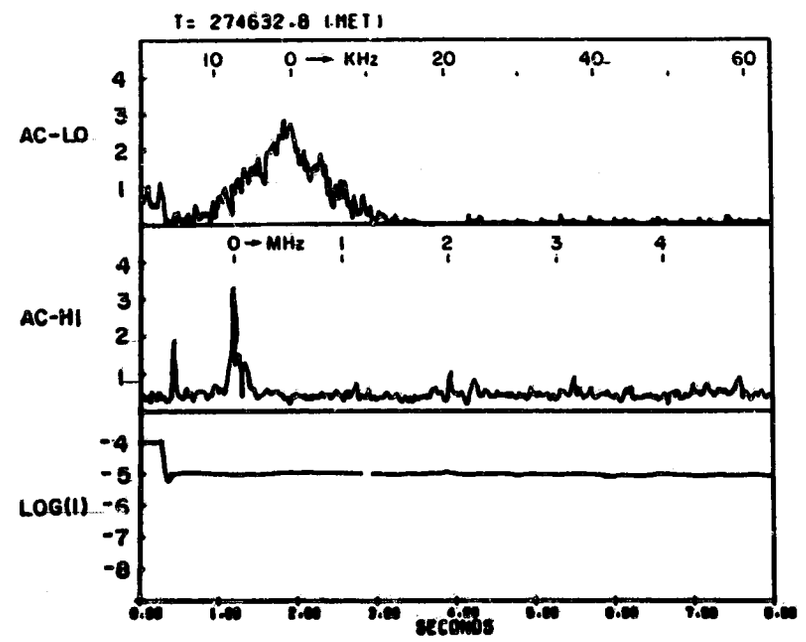

(e) Electrostatic spectra over low- and high-frequency ranges and electron current versus time. Interval 24.

Figure 8. - Continued.

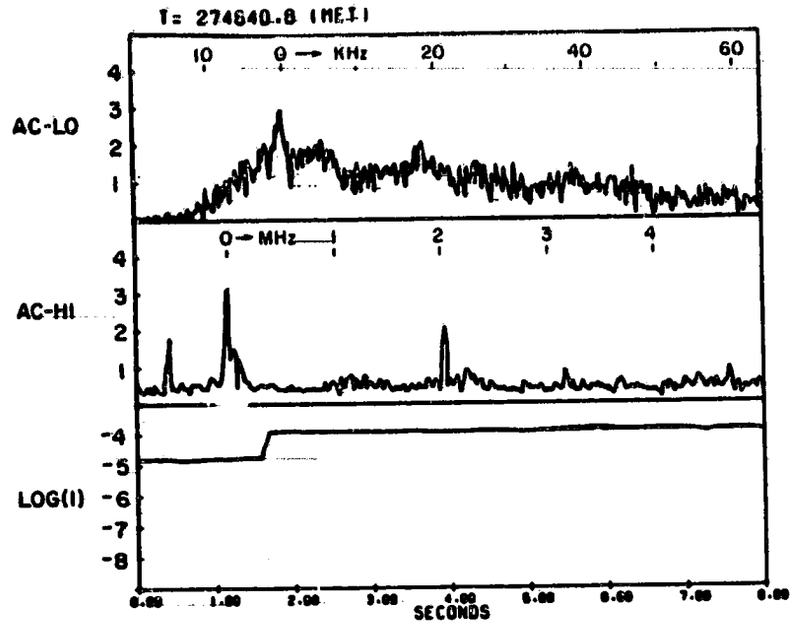

(f) Electrostatic spectra over low- and high-frequency ranges and electron current versus time. Interval 25.

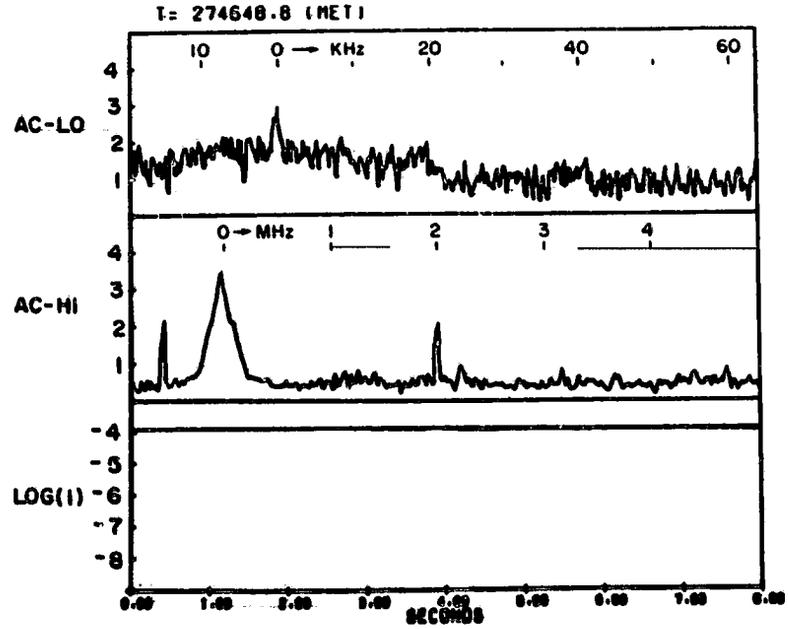

(g) Electrostatic spectra over low- and high frequency ranges and electron current versus time. Interval 26.

Figure 8. - Concluded.

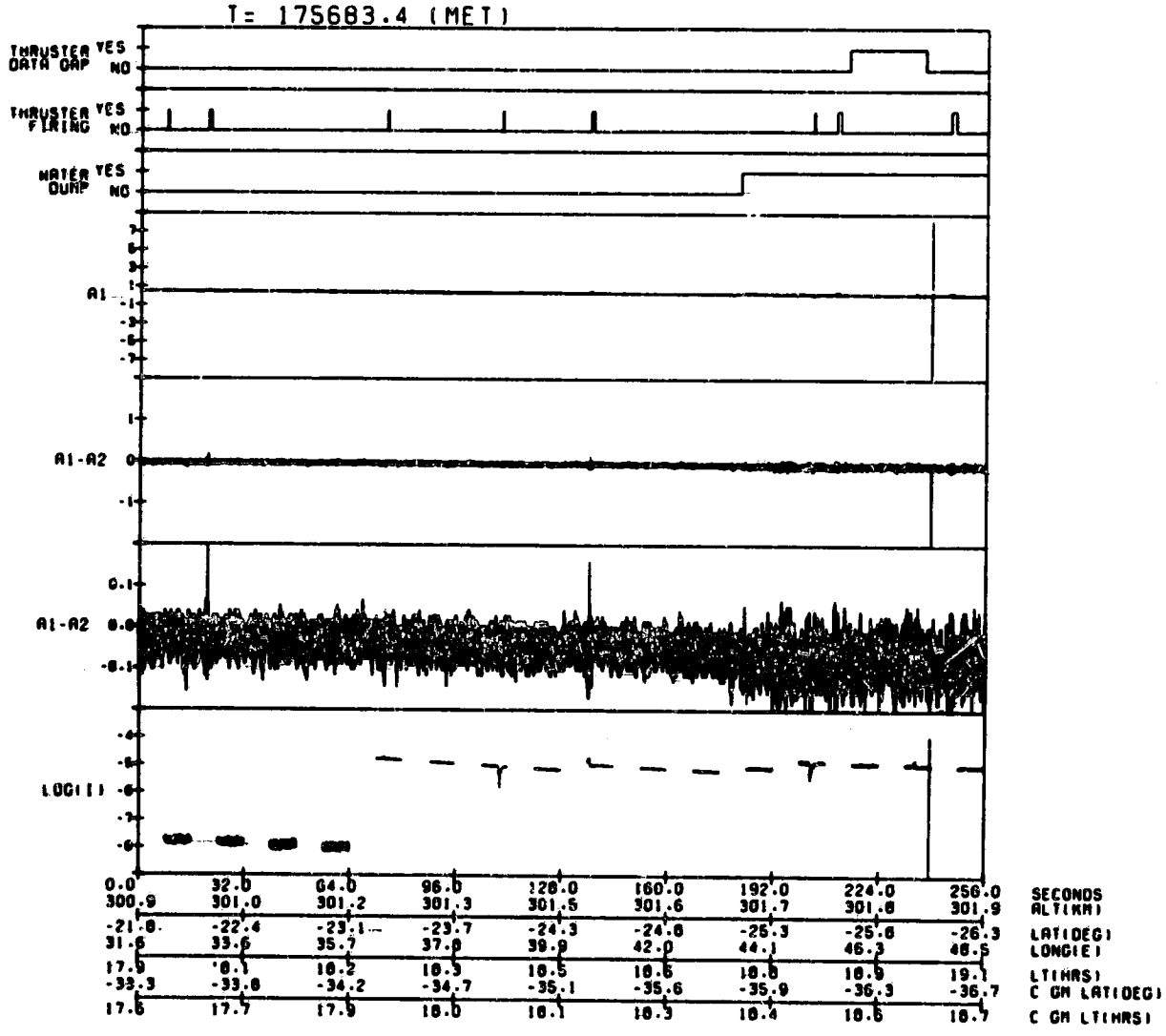

(a) Dump indicator, vehicle potential, electric field, and electron current versus time and orbital position.

Figure 9. - Water dump.

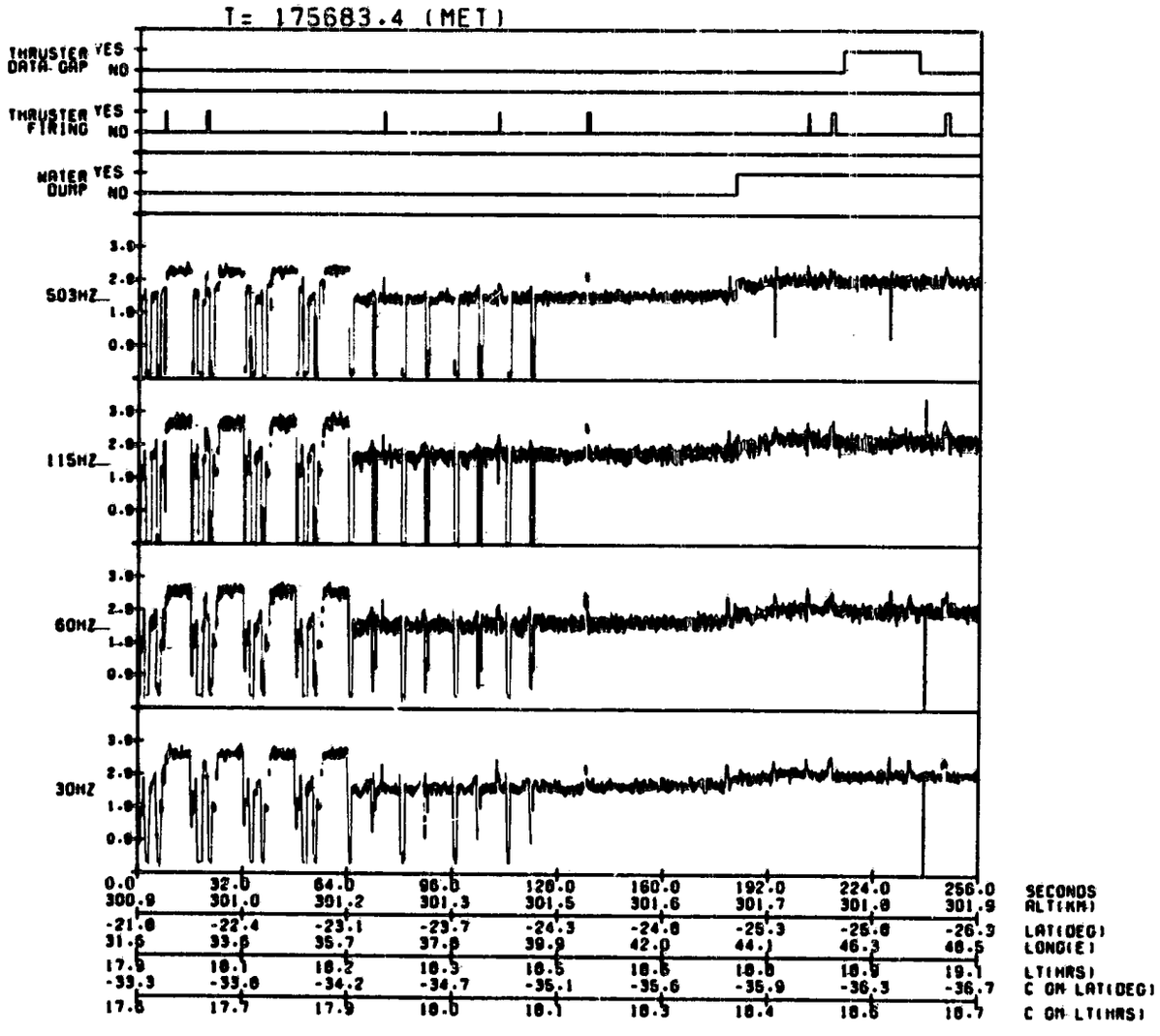

(b) Dump indicator and ΔN/N filter outputs versus time and orbital position.

Figure 9. - Continued.

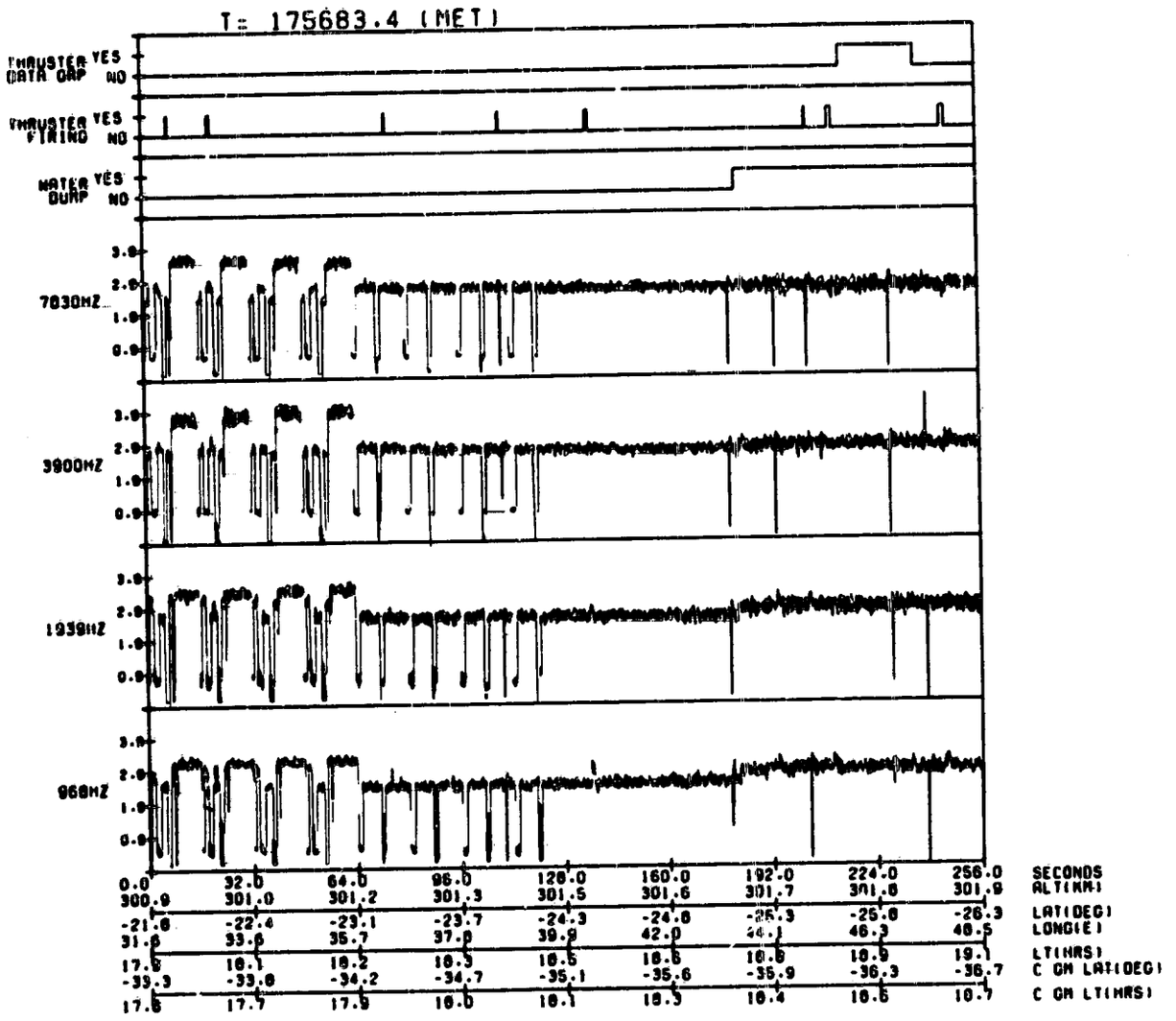

(c) Dump indicator and ΔN/N filter outputs versus time and orbital position.

Figure 9. - Continued.

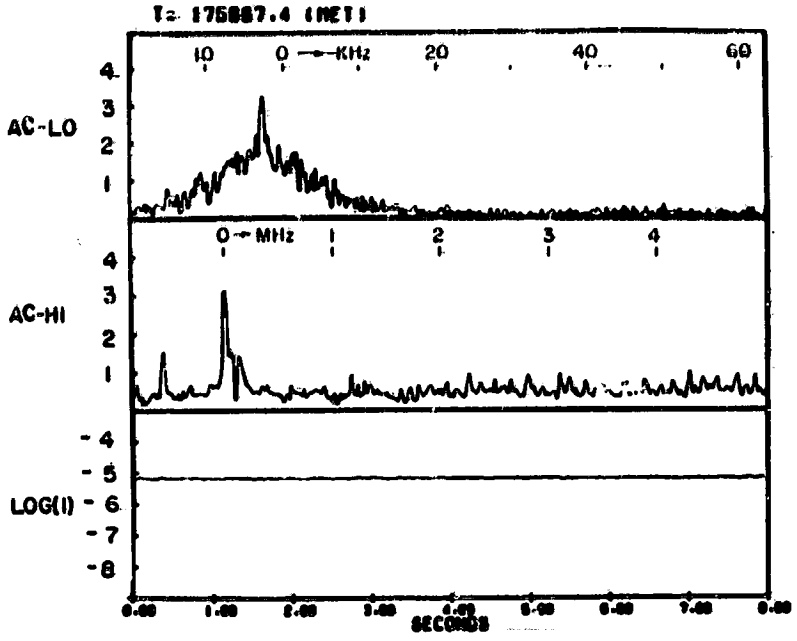

(d) Electrostatic spectra before dump versus time. Interval 22.

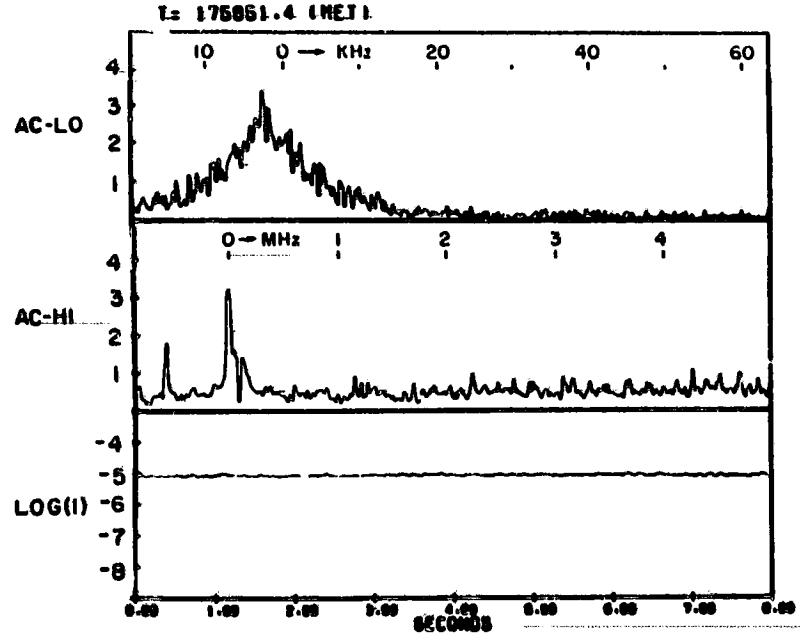

(e) Electrostatic spectra during dump versus time.

Figure 9. - Concluded.